

---

# Towards Auto-Annotation from Annotation Guidelines: *A Benchmark through 3D LiDAR Detection*

---

Yechi Ma<sup>1</sup>, Wei Hua<sup>1</sup>, Shu Kong<sup>2,3,\*</sup>

<sup>1</sup>Zhejiang University, <sup>2</sup>University of Macau, <sup>3</sup>Institute of Collaborative Innovation

## Abstract

A crucial yet under-appreciated prerequisite in machine learning solutions for real-applications is data annotation: human annotators are hired to manually label data according to detailed, expert-crafted guidelines. This is often a laborious, tedious, and costly process. To study methods for facilitating data annotation, we introduce a new benchmark *AnnoGuide: Auto-Annotation from Annotation Guidelines*. It aims to evaluate automated methods for data annotation directly from expert-defined annotation guidelines, eliminating the need for manual labeling. As a case study, we repurpose the well-established nuScenes dataset, commonly used in autonomous driving research, which provides comprehensive annotation guidelines for labeling LiDAR point clouds with 3D cuboids across 18 object classes. These guidelines include a few visual examples and textual descriptions, but no labeled 3D cuboids in LiDAR data, making this a novel task of multi-modal few-shot 3D detection without 3D annotations. The advances of powerful foundation models (FMs) make AnnoGuide especially timely, as FMs offer promising tools to tackle its challenges. We employ a conceptually straightforward pipeline that (1) utilizes open-source FMs for object detection and segmentation in RGB images, (2) projects 2D detections into 3D using known camera poses, and (3) clusters LiDAR points within the frustum of each 2D detection to generate a 3D cuboid. Starting with a non-learned solution that leverages off-the-shelf FMs, we progressively refine key components and achieve significant performance improvements, boosting 3D detection mAP from 12.1 to 21.9! Nevertheless, our results highlight that AnnoGuide remains an open and challenging problem, underscoring the urgent need for developing LiDAR-based FMs. We release our code and models at GitHub: <https://annoguide.github.io/annoguide3Dbenchmark>.

## 1 Introduction

Foundation Models (FMs) have emerged as powerful backbones that can significantly boost performance on downstream tasks when fine-tuned with carefully annotated, task-specific data [43, 26]. Data annotation remains a critical yet costly prerequisite for many real-world machine learning applications. It typically requires expert-crafted annotation guidelines, which serve as the basis for training human annotators [8]. Given the importance of annotation guidelines and the rapid advancements of FMs, we propose to investigate the task of *Auto-Annotation from Annotation Guidelines (AnnoGuide)*: automatically labeling data based on annotation guidelines by leveraging existing FMs. In particular, we explore AnnoGuide in the context of 3D detection (see Fig. 1). Addressing the AnnoGuide task not only offers practical value in reducing annotation costs but also provides a compelling benchmark for assessing how effectively current FMs can facilitate solving highly specialized, real-world problems.

---

\*Corresponding author.

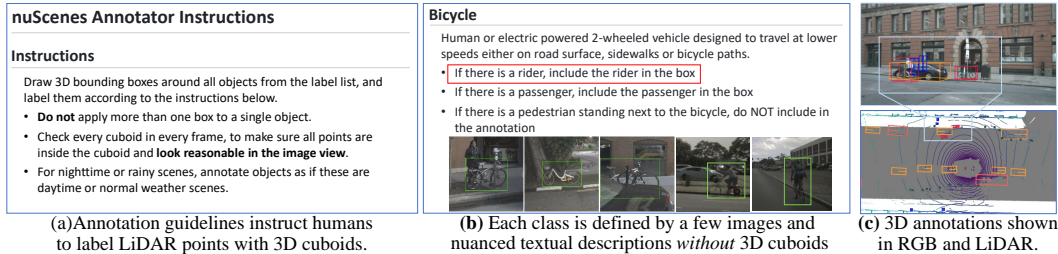


Figure 1: **Screenshots of annotation guidelines released with the nuScenes dataset** [8]. (a) The guidelines instruct human annotators to label LiDAR points with 3D cuboids for specific object classes. (b) Each object class is defined by a few visual examples and nuanced textual descriptions (ref. the red box) *without* 3D cuboid annotations. Human annotators must interpret and apply these guidelines to manually generate 3D cuboids. (c) We visualize the 3D annotations in both RGB images and the Bird’s-Eye-View (BEV) of the LiDAR point cloud.

**Status quo.** A variety of machine learning research problems are proposed to reduce the cost of data labeling, including active learning [15, 42, 20, 37, 5] and few-shot learning (FSL) [45, 7, 6, 40]. Active learning leverages the model being trained to selectively identify the most informative unlabeled samples for annotation, under the assumption that human annotators are already trained and familiar with the labeling policies. In contrast, FSL aims to train models using only a small number of labeled examples. Recent studies begin to explore FSL from the perspective of data annotation [28, 26], using annotation guidelines that include few-shot visual examples per class. However, most existing FSL works focus on relatively simple vision tasks such as image classification [26] and object detection [28], typically relying on a single FM. To advance the study of automated annotation from guidelines, we introduce a new benchmark, namely *AnnoGuide*.

**Benchmark.** We propose a benchmarking protocol of AnnoGuide through the lens of 3D detection in LiDAR data. To support this research, we repurpose the established nuScenes dataset [8] which releases annotation guidelines designed to train human annotators (Fig. 1). These guidelines define each object category using only a few visual examples and textual descriptions, *without* 3D cuboid annotations. Therefore, our AnnoGuide frames the task as *multi-modal few-shot learning for 3D detection without 3D annotation*. Compared to standard FSL tasks, AnnoGuide is significantly more challenging, although existing FSL methods can still be adapted. In particular, it calls for leveraging Large Language Models (LLMs) to interpret textual annotation guidelines, Vision-Language Models (VLMs) to detect objects defined by textual descriptions, and Vision Foundation Models (VFM) for object detection and segmentation. By combining these capabilities, AnnoGuide offers a valuable testbed for evaluating how well diverse FMs can be applied to complex, real-world annotation tasks.

**Challenges.** Our AnnoGuide presents unique and interesting challenges. First, while the goal is 3D detection in LiDAR data, the supervision for training comes from a few visual examples and textual descriptions without 3D annotations (see Fig. 1). Translating such high-level instructions into actionable supervision for machines to learn to annotate point clouds with 3D cuboids is not straightforward. Second, while it may be tempting to leverage open-source FMs, there are currently no publicly-available LiDAR-based FMs, to the best of our knowledge. This makes it non-trivial to directly apply existing FMs to LiDAR-based 3D detection. Third, given that the nuScenes annotation guidelines include both visual examples and textual descriptions, a natural formulation is to cast AnnoGuide as a *multimodal few-shot learning* problem: leveraging multiple FMs to utilize visual and textual guidance for specialized 3D detection. Despite the availability of various open-source FMs, developing an effective solution for this problem remains under-explored in the literature.

**Methodology.** By addressing the challenges outlined above, we adopt a conceptually straightforward pipeline (Fig. 2) to tackle AnnoGuide. Our approach integrates multiple FMs to (1) interpret annotation guidelines, (2) prompt foundational 2D detectors, and (3) segment object instances in RGB images. Using synchronized LiDAR and camera sensors, we lift detected object from 2D RGB frames into 3D space and generate 3D cuboids in the LiDAR point cloud as 3D detections. Further, we progressively refine key components within the pipeline, greatly boosting 3D detection performance. Despite these improvements, our comprehensive analysis shows that AnnoGuide remains far from a solved problem. We evaluate each core component and offer insights to inspire future research.

**Contributions.** We summarize our three key contributions as follows:

1. We introduce a novel and timely task, *AnnoGuide*, which not only promotes the development of practical data annotation methods but also facilitates evaluation of FMs in real-world scenarios.

2. We present a benchmarking protocol for studying AnnoGuide by repurposing the well-established nuScenes dataset. Our benchmark includes code, data, metrics, and a suite of baseline models.
3. We address AnnoGuide with a conceptually simple yet effective pipeline that integrates multiple FMs for 2D detection, segmentation, and 3D detection. We improve key components of the pipeline, greatly boosting performance and offering valuable insights to guide future research.

## 2 Related Work

**Data Annotation** is a critical yet costly prerequisite for machine learning solutions in numerous real-world applications. Abundant works are motivated to reduce annotation cost with human-in-the-loop [1, 14, 11, 34] or active learning [15, 42, 20, 37, 5]. But these works somewhat over-simplify the research problem by focusing on general object categories (e.g., car and person) [36, 39, 54, 50], without considering real-world applications that require labeling task-critical classes defined with nuanced details [28]. For instance, for autonomous driving safety, `bicycle` is defined differently [8] from what one would have thought (Fig. 1). Even the recent work [64], which studies annotation in LiDAR with RGB and VLM, also focuses on general object classes such as `car` and `motorcycle`. That said, it is an open question whether one can develop methods to automatically annotate data directly from expert-designed annotation guidelines. Our work explores this new problem AnnoGuide.

**Few-Shot Learning (FSL)** aims to reduce the cost of data annotation by developing methods to learn from a small number of labeled examples [45, 7, 6, 40]. Recent FSL methods propose to adapt a pretrained VLM [60, 61, 23, 47, 44, 17, 26]. Further, some recent works point out that FSL is better studied from a data annotation perspective: annotation guidelines contain few-shot visual examples and textual descriptions [28, 26]. However, existing work has largely focused on relatively simple tasks such as image classification [28] and object detection [26], and typically employs a single FM. In contrast, our AnnoGuide benchmark introduces a more challenging setting that requires developing multi-modal few-shot learning methods for 3D LiDAR detection without 3D annotation. Beyond its technical challenges, AnnoGuide also holds practical significance: its evaluation protocol is grounded in real-world annotation practices, making use of authentic, official annotation guidelines from the established nuScenes dataset [8] in autonomous driving research.

**Foundation Models (FMs)** are core to today’s leading AI products including GPT-4o [2], Gemini [48] and Qwen [3]. In our work, we focus on leveraging open-source Vision-Language Models (VLMs) and Visual Foundation Models (VFMs), so we briefly review key developments in them. VLMs are pretrained on large-scale image-text pairs [35, 16, 24, 25, 3], achieving unprecedented results in high-level visual understanding tasks such as visual grounding, image captioning, and visual question answering. VFMs, by contrast, are trained primarily on visual data [10, 9, 63, 29, 49] and excel at perception tasks such as object detection [58, 25, 38, 25] and segmentation [19, 51]. Recent efforts have attempted to transfer the general perception abilities of VLMs to LiDAR-based perception by associating VLM output with LiDAR points through geometric alignment between camera and LiDAR sensors [18, 30]. However, such approaches fall short in domains like autonomous driving, where object definitions require nuanced understanding critical to safety [28]. Therefore, adapting FMs effectively to address real-world, task-specific challenges is essential [28, 26]. Our work evaluates FMs through a highly-specialized yet widely-studied task: 3D LiDAR detection.

FMs are evaluated across a wide range of tasks such as mathematical reasoning [27], low-level visual understanding [56] and high-level language reasoning [62]. Our AnnoGuide benchmark extends this evaluation to 3D perception in the context of autonomous driving, motivated from the perspective of real-world data annotation practices. To the best of our knowledge, there is currently no FM specifically designed for LiDAR-based perception. Therefore, our AnnoGuide benchmark evaluates the performance of combinations of existing FMs through our proposed methods. Our results reveal significant room for improvement in adapting FMs over annotation guidelines to meet the demands of highly-specialized 3D perception tasks.

**3D LiDAR Detection** has been extensively studied in autonomous driving research, leading to the release of several large-scale datasets such as nuScenes [8], KITTI [12], Waymo [46], and Argoverse2 [53]. Among them, nuScenes is the only one that releases its official annotation guidelines. Most methods train 3D detectors over massive annotated LiDAR data, optionally with annotated RGB frames [57, 4, 21]; some build 3D LiDAR detection in a zero-shot manner [59, 55]. These methods typically focus on detecting common object classes (e.g., `vehicle`, `pedestrian` and `cyclist`)

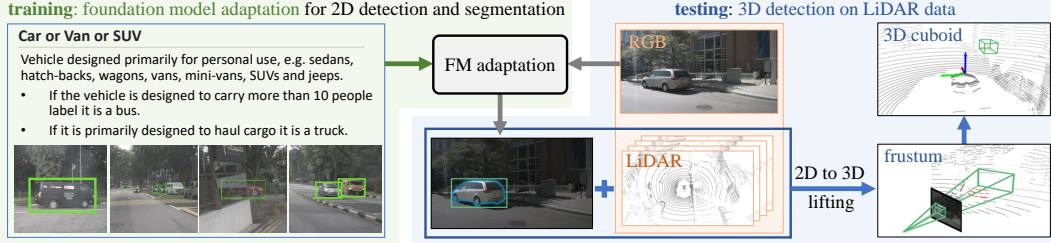


Figure 2: We adopt a pipeline to solve AnnoGuide by adapting open-source foundation models (FMs). Specifically, over the visual examples and textual descriptions that define object classes of interest, we adapt a Vision-Language Model (VLM) and a Vision Foundation Model (VFM) for object detection and segmentation. The adapted FMs produce decent 2D detections on unlabeled RGB frames. With the aligned LiDAR and RGB frames, we lift each 2D detection to 3D, locate corresponding LiDAR points, and generate a 3D cuboid as the 3D detection. We delve into FM adaption and 3D cuboid generation, and improve them in this work (Section 4).

and neglecting rare yet safety-critical ones, despite that annotation guidelines have defined all such classes [33]. Our AnnoGuide benchmark evaluates performance across all defined classes. Notable, our work assesses multi-modal few-shot learning approaches for 3D detection without 3D annotations.

### 3 Problem Formulation and Benchmarking Protocol

**Problem Formulation.** In plain terms, our AnnoGuide mimicks human annotators to label LiDAR data using 3D cuboids. As the annotation guidelines (Fig. 1) contain only textual descriptions and a few 2D visual examples without reference 3D cuboids, any developed methods must learn from the visual and textual information to generate 3D cuboids on the LiDAR data. Similar to human annotators, the developed methods are expected to (1) understand textual descriptions of object categories with the help of visual examples, (2) detect objects in RGB frames and associate LiDAR points to them, (3) utilize prior knowledge about objects’ 3D shapes and sizes to generate appropriate 3D cuboids in the LiDAR point cloud. We evaluate methods primarily on 3D LiDAR detection quality. For methods that generate 2D detections as intermediate outputs (mirroring human annotators’ workflow), we also assess their 2D detection performance.

**Dataset.** We repurpose the nuScenes dataset [8] which is publicly available under the CC BY-NC-SA 4.0 license. The dataset provides annotations for 18 classes. While the official nuScenes annotation guidelines contain visual examples (Fig. 1), we do not use them in our benchmark but instead select 4-8 RGB images for each class from the nuScenes training set. The reason is that the visual examples in the original guidelines are non-nuScenes images (likely sourced from the Internet), which introduce domain gaps and potential copyright concerns. We meticulously select the images that clearly capture visual signatures of each class, simulating iconic visual examples used in annotation guidelines. For each selected image, we retain only the annotations of the target class, discarding others. For example, Fig. 3 shows selected frames for *police officer* class, where objects like *car* and *traffic cone* are present but not annotated. We consider this federated dataset [28], along with textual descriptions in the nuScenes guidelines, as the training set in our AnnoGuide benchmark. It is worth noting that, while our AnnoGuide focuses on 3D detection in LiDAR data, the nuScenes annotation guidelines do not provide 3D cuboid annotations for demonstration. Lastly, from the nuScenes’ official validation set (containing 6,019 annotated LiDAR sweeps and 36,114 annotated RGB frames), we sample 570 frames as our validation set for hyperparameter tuning and model selection. This small validation set simulates the expert-in-the-loop quality control, where domain experts typically oversee annotation progress and quality. For benchmarking, we use the nuScenes’ official validation set as our test set. We release the data splits in our codebase at GitHub.

**Metrics.** We evaluate methods w.r.t both 2D detection and 3D detection metrics:

- *2D metrics.* Following [22], we report mean Average Precision which is the mean of per-class AP at IoU=0.5. We denote this metric as  $mAP^{2D}$ .
- *3D metrics.* Following nuScenes [8], we first report mean Average Precision over per-class AP at different ground-plane distance thresholds, [0.5, 1.0, 2.0, 4.0] in meters. We denote this metric as  $mAP^{3D}$ . We also report the nuScenes Detection Score (NDS), which summarizes translation error, scale error, orientation error, velocity error, and attribute error.

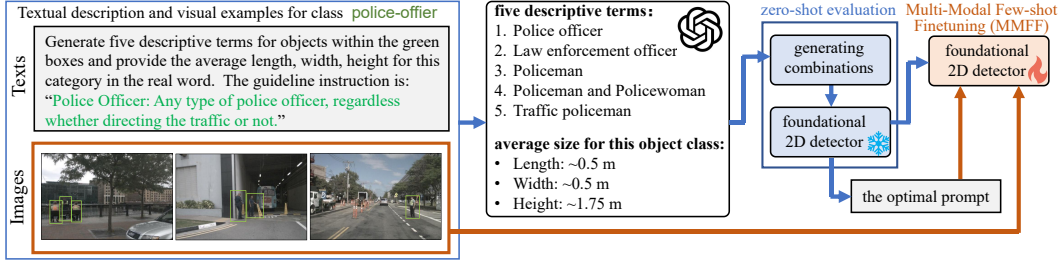


Figure 3: For each targeted class name, we use a pretrained VLM (GPT-4o [2] in this work) to find a list of terms that match the textual description and visual examples provided in the annotation guidelines. We then test each term and its combinations to search the best one that maximizes the zero-shot detection performance of a foundational object detector (GroundingDINO [25] in this work) on the validation set. We use the best term (or term combination) to finetune the foundational detector, yielding notable improved performance (Table 1).

## 4 Methodology: Lifting 2D Detections to 3D

We adopt the framework for 3D detection by lifting 2D detections, as illustrated in Fig. 2. The pipeline has two key components: (1) 2D object detection on RGB frames, and (2) 3D cuboid generation for each detected object by using its associated LiDAR points. We describe them and improvements in Section 4.1 and 4.2 respectively, and a few more technical enhancements in Section 4.3.

### 4.1 2D Detection by Multi-Modal Few-Shot Finetuning

For 2D detection on RGB frames, we exploit an open-source foundational detector. Foundational detectors yield impressive zero-shot detection performance on natural images but they are not tailored to specific tasks [28]. For example, in the nuScenes dataset for autonomous driving, `bicycle` is defined differently from commonsense (Fig. 1): annotators should include the rider (when existing) in the box annotation. Nevertheless, we start with the off-the-shelf GroundingDINO [25] as a baseline. We present improved methods next.

**Prompt Engineering** means designing prompts that can lead to better zero-shot performance [31, 32]. This is often done manually, but in this work, we use an automated method to generate better prompts for object detection (Fig. 3). Specifically, for each object class, we prompt a VLM to find five descriptive terms that fit the textual descriptions and visual examples provided in the guidelines. Then, we test each term or any combination to prompt GroundingDINO for zero-shot detection. We pick the term (or combined terms) that yields the highest 2D detection precision on the validation set, and use it to prompt GroundingDINO for object detection on unlabeled RGB frames.

**Multi-Modal Few-Shot Finetuning.** As a few visual examples are available in the annotation guidelines, we use them as few-shot training examples (which have box annotations as ground-truth labels) to finetune the foundational detector (Fig. 3). It is worth noting visual examples in the guidelines are annotated in a federated way, i.e., all objects belong to the focused class are annotated while others are not. Therefore, when finetuning GroundingDINO on the few-shot images, we compute the loss over specific classes pertaining to the images without treating detections of other classes as false positives. We compare finetuned models using either the original class name or the selected terms (presented above), and find that the latter performs better (Table 1).

### 4.2 3D Cuboid Generation by Multi-Hypothesis Testing

For each detection obtained above, we construct a frustum and identify LiDAR points therein (ref. bottom-right of Fig. 2). Over these points, we generate a proper 3D cuboid as the 3D detection. Specifically, for a given detected object, we use the size prior based on its predicted class (ref. Fig. 3) and the identified LiDAR points to generate a 3D cuboid as the 3D detection.

**Background Points Removal via Foreground Segmentation.** LiDAR points within the detection box may include background points, particularly near the box boundaries. To address this, we perform foreground segmentation to precisely segment the object within the detection box. We use the foundational segmentation model SAM [19] by prompting it with the 2D detection box. Fig. 4 and 5 display segmentation results, demonstrating the effectiveness in refining LiDAR point selection. Previous works have used LiDAR points and foreground segmentation to lift 2D detections

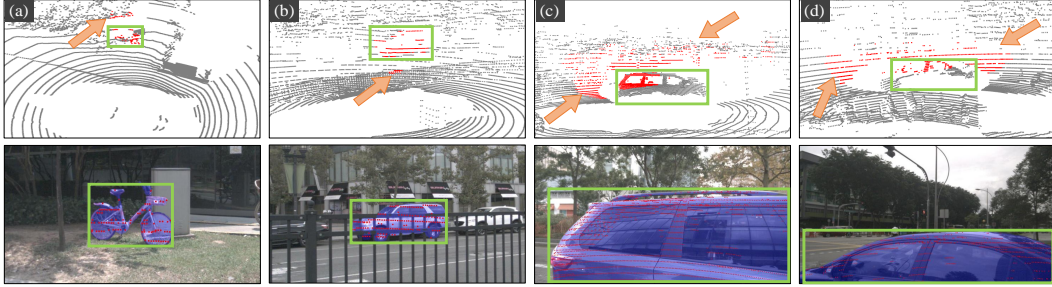


Figure 4: Generating a 3D cuboid based on LiDAR points is challenging as points can be from occluders and backgrounds. For example, (a) LiDAR points projected on a bicycle can be from background through wheels; (b) points projected on a car can be from a fence occluding the car; (c-d) points projected on a car can be background through the windows and windshield of the car.

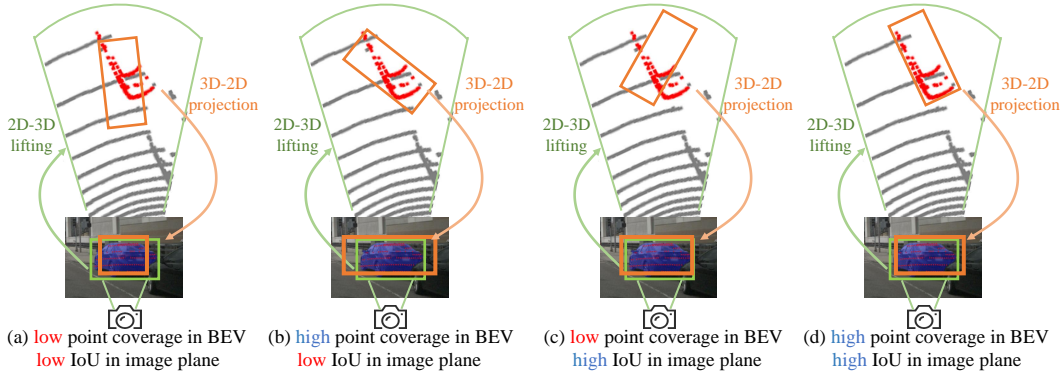


Figure 5: We generate a 3D cuboid for the 2D detected object through Multi-Hypothesis Testing (MHT). In the frustum projected from the 2D detection, we locate the LiDAR points that lie in the mask of the 2D detected object (when projected from 3D to 2D image plane). For the recognized car, we use the prior size obtained by prompting GPT-4o (ref. Fig. 2) to fit the LiDAR points in 3D BEV. We define a list of angular rotations and translation step sizes to measure their point coverage in BEV and IoU on the image plane, and find the best-fitting one that yields the highest point coverage and IoU. Our method outperforms existing ones (Table 2).

to 3D [54, 18, 64] but overlooked critical challenges — the remaining LiDAR points can still come from occluders (e.g., a fence in front of a vehicle) and background artifacts (e.g., points on a wall visible through a vehicle’s windshield and windows), as shown in Fig. 4. We propose a method to mitigate these issues via Multi-Hypothesis Testing (MHT), as detailed next.

**3D Cuboid Generation via MHT.** Following the nuScenes annotation guidelines, human annotators manually fit 3D cuboids to enclose LiDAR points belonging to objects identified in 2D images. We automate this process through an MHT-based approach for 3D cuboid generation, as illustrated in Fig. 5. For a 2D detection, we first determine the cuboid dimensions using the predicted class label by the 2D detector and the average size prior obtained from GPT-4o (Fig. 3). We translate and rotate this cuboid within the frustum using predefined rotation angles and translation step sizes. We select the optimal cuboid based on two criteria: (1) maximal coverage of LiDAR points within the cuboid, and (2) highest Intersection-over-Union (IoU) between the original 2D detection box and the projected 2D box of the 3D cuboid. We provide more implementation details in Appendix F.

### 4.3 More Technical Enhancements

We incorporate a few more techniques to improve 3D cuboid generation and elaborate on them below.

**LiDAR Sweep Aggregation.** As a single LiDAR sweep can be too sparse to precisely localize objects in 3D, we aggregate multiple sweeps. While existing methods typically aggregate *history* sweeps for 3D detection at a given timestamp, we can also aggregate *future* sweeps to facilitate data annotation. We analyze per-category 3D detection performance w.r.t different aggregation strategies (Table 3) and find that aggregation strategies significantly impact detection accuracy for certain classes.

**3D Cuboid Scoring with Geometric Cues.** We score each generated 3D cuboid using both the 2D detection confidence  $S_{2D}$  and 3D geometric information. To capture 3D geometric cues, we compute

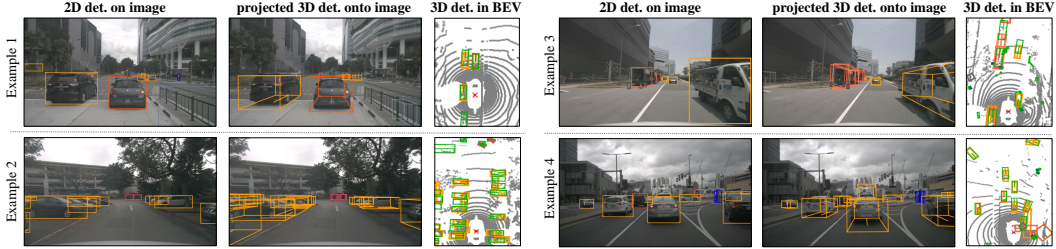


Figure 6: **Visualization of detection results on four testing examples.** For each example, we display 2D detections, and 3D detections (i.e., the generated 3D cuboids) projected onto the RGB image and the BEV of LiDAR data. Visual results show that our method decently detects objects that are in far field and small in size, which are usually challenging to detect [33, 13]. We provide more visual results in the Appendix H.

Table 1: Different strategies of finetuning foundational 2D detectors yield different 3D detection performances. For 3D cuboid generation, we use CM3D [18]. Recall that we refine class names using an off-the-shelf VLM (Fig. 3). With the GroundingDINO (GD) 2D detector, replacing the original class names (“o-name”) with refined class names (“r-name”) yields better zero-shot detection performance. Importantly, finetuning GD (fit-GD) using r-name performs the best. Table 7 in the Supplement lists details.

	GD o-name	fit-GD o-name	GD r-name	fit-GD r-name
mAP <sup>2D</sup>	16.9	20.0	18.2	<b>20.8</b>
mAP <sup>3D</sup>	12.1	16.6	15.7	<b>18.2</b>
NDS	16.6	21.2	22.1	<b>23.1</b>

Table 2: We compare different 3D cuboid generation methods, including our heuristic baseline, CM3D [18], a 3D detector CenterPoint (CP) [57] trained on the Argoverse2 LiDAR data [52], and our MHT-based method. Surprisingly, the trained 3D detector CP yields poor performance. We believe the reason is the discrepancy between LiDAR models of the nuScenes and Argoverse2 datasets. We compare the specifics of the LiDAR models in Table 8 of the Supplement. Our MHT-based method (Fig. 5) performs the best. Table 9 in the Supplement lists more details.

	CM3D [18]	CP [57]	MHT
mAP <sup>3D</sup>	18.2	3.6	<b>19.2</b>
NDS	23.1	19.0	<b>23.8</b>

an occupancy rate [55] based on LiDAR point distribution within the cuboid. Specifically, we (1) project the 3D cuboid onto the ground plane, obtaining a BEV rectangle, (2) discretize this rectangle into a  $7 \times 7$  grid, (3) count grid cells ( $N$ ) containing at least one project LiDAR point, and (4) compute the occupancy rate as  $S_{3D} = N/49$ . The final cuboid score combines these metrics through weighted summation:  $S_{2D}$  and  $S_{3D}$ , i.e.,  $S = \alpha * S_{2D} + (1 - \alpha) * S_{3D}$ , where the weighting parameter  $\alpha$  is optimized to maximize 3D detection precision on the validation set.

**Tracking-Based Score Refinement.** To refine the scores of generated 3D cuboids at a given timestamp, we leverage temporal information by “tracking” objects across LiDAR sweeps. Concretely, we adopt a heuristic approach to associate 3D cuboids which have the same class labels (predicted by the 2D detector) and are spatially close. For all the 3D cuboids belong to the same track, we replace their individual scores with their mean score. Despite the simplicity of this method, our experiments demonstrate that it remarkably improves 3D detection performance (Table 4).

## 5 Experimental Results and Analysis

We conduct a series of experiments to validate the effectiveness (Fig. 6) of our methods and demonstrate the challenges in AnnoGuide. We start by introducing important implementation details.

**Implementations.** We exploit four FMs in this work: the GPT-4o [2] for annotation guidelines understanding, the VLM GroundingDINO as a 2D detector [25], and the VFM SAM [19] for object segmentation. When operating with FMs, we use an NVIDIA A6000 GPU. We use Python and PyTorch in experiments. We provide more details about FM adaptation in the Supplement (Section K) and release our code and models at GitHub.

**Analysis on 2D detection.** We analyze 2D detection performance of using different finetuning methods to adapt the foundational detector GroundingDINO. As nuScenes dataset [8] does not provide 2D box annotations on RGB images, we project the 3D-cuboid annotations onto the image plane using camera parameters to generate 2D-box annotations. We compare different methods: (1) using the original class names to prompt GroundingDINO for zero-shot detection (dubbed “GD w/ o-name”), (2) finetuning GroundingDINO using the few-shot examples provided in the annotation

Table 3: **Analysis of sweep aggregation strategies on per-class 3D detection performance** (mAP<sup>3D</sup>). “ $P+C+F$ ” denotes aggregating the past  $P$  sweeps, the current sweep  $C$ , and the future  $N$  sweeps; we drop  $P$  or  $F$  if not aggregating any past or future sweeps. In each row, we bold the highest number and highlight it if exceeding other numbers by 0.5 points. Somewhat surprisingly, aggregation strategies greatly impacts performance on certain classes, e.g., `construction-worker`, `bicycle` and `traffic-cone`, aggregating the past 2 sweeps yields remarkably better performance than other strategies.

Class	10+C	6+C	2+C	C	C+2	C+6	C+10	1+C+1	3+C+3	5+C+5
car	25.6	27.4	29.1	<b>30.0</b>	29.8	28.6	27.1	29.9	28.8	28.1
truck	14.0	14.6	<b>15.5</b>	15.4	15.4	15.0	14.3	<b>15.5</b>	15.3	14.9
trailer	1.7	1.7	1.7	1.7	1.7	1.7	1.7	1.7	1.7	1.7
bus	11.1	11.9	13.0	<b>14.0</b>	13.1	12.6	12.0	13.3	12.5	11.9
construction-vehicle	8.8	9.2	9.5	9.5	9.5	9.4	9.1	9.5	9.6	9.4
bicycle	22.5	24.9	28.5	30.1	<b>32.4</b>	28.9	26.6	29.3	29.3	28.4
motorcycle	37.6	42.2	48.5	50.7	49.6	43.6	38.0	<b>51.2</b>	48.6	45.5
emergency-vehicle	4.5	4.6	4.3	<b>5.4</b>	4.5	4.4	4.1	5.2	4.0	3.9
adult	34.5	43.6	56.1	58.8	59.8	46.5	36.1	<b>60.7</b>	56.3	49.1
child	4.2	<b>5.1</b>	4.6	3.5	2.8	2.6	1.9	3.6	2.9	2.7
police-officer	1.2	1.5	2.2	2.2	2.2	2.0	1.8	<b>2.3</b>	2.0	1.9
construction-worker	13.6	16.3	22.9	25.6	<b>28.6</b>	24.3	20.5	27.9	25.1	22.3
stroller	19.2	20.2	21.5	21.5	23.3	24.1	<b>24.2</b>	21.7	21.5	23.2
personal-mobility	6.6	9.1	8.8	8.7	9.1	6.9	6.9	<b>10.4</b>	8.6	8.6
pushable-pullable	4.6	4.7	4.7	4.8	<b>5.0</b>	4.8	4.8	4.8	4.8	4.8
debris	0.1	0.1	0.1	0.1	0.1	0.1	0.1	0.1	0.1	0.1
traffic-cone	44.3	46.7	50.2	52.0	<b>54.0</b>	51.3	48.4	53.1	52.0	50.1
barrier	11.3	11.4	11.5	11.5	11.5	11.5	11.5	11.5	11.5	11.5

guidelines and the original class names (dubbed “ft-GD w/ o-name”), (3) using GPT-4o to refine class names and prompt GroundingDINO with the refined names (dubbed “GD w/ r-name”), and (4) finetuning GroundingDINO using the few-shot examples provided in the annotation guidelines and the refined class names (dubbed “ft-GD w/ r-name”). Table 1 lists the results, showing that “ft-GD w/ r-name” performs the best. The results demonstrate that refining class names, e.g., from `police-officer` to “law enforcement officer” (details in Supplement), facilitates FM adaptation.

**Analysis on 3D cuboid generation.** We compare different 3D cuboid generation methods: CM3D proposed in [18] and our MHT-based method (Section 4.2). Note that we also compare a 3D detector CenterPoint trained on another dataset Argoverse2 [52], intending to demonstrate the challenge of training a LiDAR-based detector on LiDAR data collected using a different LiDAR model (see details in Section D of the Supplement). Table 2 lists the results, demonstrating that our MHT-based method performs the best. Interestingly, the 3D detector CenterPoint significantly underperforms other methods, although we carefully tuned hyperparameters and unified Argoverse2 LiDAR data format with nuScenes. We believe the reason lies in the different LiDAR models used in the two datasets, causing discrepancies in terms of point density, vertical FOV, scan frequency, resolution, etc. This suggests that developing LiDAR-based foundation models is both challenging.

**Analysis of LiDAR sweep aggregation.** We report per-class detection accuracy by applying different aggregation strategies. Table 3 shows that aggregating the past and/or future sweeps improves on most classes. Interestingly, results are not “symmetric”, possibly due to their motion patterns: for `traffic-cone`, `construction-worker` and `bicycle`, aggregating the future two sweeps yields significantly better performance than aggregating the past two sweeps; for `child`, aggregating the past 6 sweeps is significantly better than other strategies!

**Assembling the pieces.** In our pipeline (Fig. 2), we include the proposed techniques, including the MHT-based 3D cuboid generation, class-aware Sweep Aggregation, geometry-based auxiliary scoring method, and tracking-based score refinement. Table 4 shows how each technique brings 0.7~1.9% 3D mAP improvements, and using them all yields 3.7% 3D mAP gains. Despite the remarkable improvements, it is also clear that the task AnnoGuide is quite challenging that the overall 3D mAP (21.9) is far from comparable to the results of supervised learned 3D detectors, e.g., [33] reports 43.6 mAP on the 18 classes of nuScenes.

**Does few-shot learning for 3D cuboid refinement work?** To answer this, we assume access to 3D cuboid annotations on LiDAR data corresponding to the visual examples in the annotation guidelines. We train a network on the “few-shot” 3D labeled data, which takes generated 3D cuboids as input and predicts offsets to refine their location, size, orientation and quality score. Despite careful tuning of the network architecture and hyperparameters (details in Section H of the Supplement), the model

Table 4: **Our proposed techniques improve 3D cuboid generation** (Section 4.2). The first row shows results of a method that adopts our finetuned GroundingDINO for 2D detection and CM3D [18] for 3D cuboid generation. MHT stands for Multi-Hypothesis Testing for 3D cuboid generation; “SA.” uses class-aware sweep aggregation (Table 3);  $S_{3D}$  incorporates 3D geometric cues to score generated 3D cuboids; “track” means using 3D tracks to refine scores of generated cuboids. Results demonstrate the effectiveness of each technique in improving 3D cuboid generation.

<i>MHT</i>	<i>SA.</i>	$S_{3D}$	<i>track</i>	mAP <sup>3D</sup>	NDS
				18.2	23.1
✓				19.2	23.8
✓	✓			20.1	24.3
✓	✓	✓		20.8	24.6
✓	✓	✓	✓	<b>21.9</b>	<b>25.0</b>

Table 5: **Analysis of learning to refine generated 3D cuboids.** Suppose we manually prepare 3D cuboids on the LiDAR point clouds for the visual examples provided in the annotation guidelines. We use them to learn a model that takes as input a generated 3D cuboid and output refined cuboid. The refinement can translate the cuboid through re-centering, adjust cuboid *size*, tune the *orientation*, and re-score the cuboid. We tune the model over the validation set. Results show that learning to refine the size of generated cuboids on limited examples is beneficial.

<i>center</i>	<i>size</i>	<i>orientation</i>	<i>score</i>	mAP <sup>3D</sup>	NDS
				21.9	25.0
✓				20.8	21.9
	✓			21.9	<b>26.4</b>
		✓		21.9	24.7
	✓	✓		21.9	25.9
			✓	20.3	21.2

yields only a small improvement of 1.4 NDS (Table 5). We hypothesize that the scarcity of 3D labeled data poses significant challenges for training a 3D perception model. The results, together with Table 2, suggest that a LiDAR-based FM could substantially advance LiDAR perception.

## 6 Discussions on Broader Impacts and Limitations

**Broader Impacts.** Our AnnoGuide benchmark offers a new venue where various foundational models can be accessed in multiple aspects with the final goal of 3D LiDAR detection, e.g., understanding textual descriptions in annotation guidelines, summarizing core information from texts and visual examples, generalizing to specific object classes for precise detection, etc. Our benchmark can facilitate the development of methods for automating data annotation by learning from expert-crafted guidelines. The developed methods can benefit real-world applications which adopt machine learning solutions, where data annotation is typically a prerequisite. Such applications span industry, health care, interdisciplinary research, etc. In the meanwhile, insights, philosophical thoughts and techniques delivered in this work may potentially inspire dataset curation and methods for malicious attacks for specific applications. These could be negative impacts.

**Limitations.** We note several limitations. First, while our pipeline demonstrates promising results, its real-world applicability for data annotation requires further comprehensive validation. Second, our methods do not leverage unlabeled data, which could be exploited through semi-supervised learning to enhance FM adaptation for AnnoGuide. Third, we rely on per-category size priors; adapting these priors to individual instances could further improve performance. Fourth, our tracking-based score refinement focuses on cuboid confidence but could also be used for optimizing cuboid orientation or velocity, which are key factors for autonomous driving and evaluation metrics like NDS. Fifth, our 3D cuboid generation operates on isolated object instances, but incorporating contextual and proxemic relationships between objects could yield additional gains. Finally, our work does not attempt to build a LiDAR-based foundation model, a critical yet underexplored direction for future research.

## 7 Conclusion

We introduce *AnnoGuide*, a novel and timely benchmark for *Auto-Annotation from Annotation Guidelines*. AnnoGuide simulates real-world data annotation pipelines, where human annotators learn to annotate unlabeled data for specific object classes using expert-designed guidelines. We study AnnoGuide through 3D LiDAR detection by repurposing the nuScenes dataset. Notably, despite its focus on 3D detection, the nuScenes annotation guidelines do not provide 3D annotations, making AnnoGuide particularly challenging. To approach AnnoGuide, we propose simple yet effective methods, including *Multi-Modal Few-Shot Finetuning* and *Multi-Hypothesis Testing-based 3D cuboid generation*, which remarkably improve 3D detection performance over baseline approaches. However, our results demonstrate that the AnnoGuide benchmark remains far from solved, highlighting the need for further research, e.g., developing LiDAR-based foundation models.

## Acknowledgements

This work was supported by FDCT (0067/2024/ITP2), the University of Macau (SRG2023-00044-FST), and the Institute of Collaborative Innovation. Authors thank Neehar Peri for insightful discussions, and Shuoquan Wei for running 2D detectors.

## References

- [1] Azad Abad, Moin Nabi, and Alessandro Moschitti. Autonomous crowdsourcing through human-machine collaborative learning. In *Proceedings of the 40th International ACM SIGIR Conference on Research and Development in Information Retrieval*, pages 873–876, 2017.
- [2] Josh Achiam, Steven Adler, Sandhini Agarwal, Lama Ahmad, Ilge Akkaya, Florencia Leoni Aleman, Diogo Almeida, Janko Altenschmidt, Sam Altman, Shyamal Anadkat, et al. Gpt-4 technical report. *arXiv preprint arXiv:2303.08774*, 2023.
- [3] Jinze Bai, Shuai Bai, Yunfei Chu, Zeyu Cui, Kai Dang, Xiaodong Deng, Yang Fan, Wenbin Ge, Yu Han, Fei Huang, Binyuan Hui, Luo Ji, Mei Li, Junyang Lin, Runji Lin, Dayiheng Liu, Gao Liu, Chengqiang Lu, Keming Lu, Jianxin Ma, Rui Men, Xingzhang Ren, Xuancheng Ren, Chuanqi Tan, Sinan Tan, Jianhong Tu, Peng Wang, Shijie Wang, Wei Wang, Shengguang Wu, Benfeng Xu, Jin Xu, An Yang, Hao Yang, Jian Yang, Shusheng Yang, Yang Yao, Bowen Yu, Hongyi Yuan, Zheng Yuan, Jianwei Zhang, Xingxuan Zhang, Yichang Zhang, Zhenru Zhang, Chang Zhou, Jingren Zhou, Xiaohuan Zhou, and Tianhang Zhu. Qwen technical report. *arXiv preprint arXiv:2309.16609*, 2023.
- [4] Xuyang Bai, Zeyu Hu, Xinge Zhu, Qingqiu Huang, Yilun Chen, Hongbo Fu, and Chiew-Lan Tai. Transfusion: Robust lidar-camera fusion for 3d object detection with transformers. In *IEEE/CVF Conference on Computer Vision and Pattern Recognition (CVPR)*, 2022.
- [5] Jihwan Bang, Sumyeong Ahn, and Jae-Gil Lee. Active prompt learning in vision language models. In *IEEE/CVF Conference on Computer Vision and Pattern Recognition (CVPR)*, pages 27004–27014, 2024.
- [6] Peyman Bateni, Raghav Goyal, Vaden Masrani, Frank Wood, and Leonid Sigal. Improved few-shot visual classification. In *IEEE/CVF Conference on Computer Vision and Pattern Recognition (CVPR)*, 2020.
- [7] Malik Boudiaf, Imtiaz Ziko, Jérôme Rony, José Dolz, Pablo Piantanida, and Ismail Ben Ayed. Information maximization for few-shot learning. *Advances in Neural Information Processing Systems (NeurIPS)*, 2020.
- [8] Holger Caesar, Varun Bankiti, Alex H Lang, Sourabh Vora, Venice Erin Liong, Qiang Xu, Anush Krishnan, Yu Pan, Giancarlo Baldan, and Oscar Beijbom. nuscenes: A multimodal dataset for autonomous driving. In *IEEE/CVF Conference on Computer Vision and Pattern Recognition (CVPR)*, 2020.
- [9] Mathilde Caron, Hugo Touvron, Ishan Misra, Hervé Jégou, Julien Mairal, Piotr Bojanowski, and Armand Joulin. Emerging properties in self-supervised vision transformers. In *IEEE/CVF International Conference on Computer Vision (ICCV)*, 2021.
- [10] Ting Chen, Simon Kornblith, Mohammad Norouzi, and Geoffrey Hinton. A simple framework for contrastive learning of visual representations. In *International conference on machine learning*, pages 1597–1607. PMLR, 2020.
- [11] Ho Kei Cheng, Yu-Wing Tai, and Chi-Keung Tang. Modular interactive video object segmentation: Interaction-to-mask, propagation and difference-aware fusion. In *IEEE/CVF Conference on Computer Vision and Pattern Recognition (CVPR)*, pages 5559–5568, 2021.
- [12] Andreas Geiger, Philip Lenz, Christoph Stiller, and Raquel Urtasun. Vision meets robotics: The kitti dataset. *The international journal of robotics research*, 32(11):1231–1237, 2013.
- [13] Shubham Gupta, Jeet Kanjani, Mengtian Li, Francesco Ferroni, James Hays, Deva Ramanan, and Shu Kong. Far3det: Towards far-field 3d detection. In *IEEE/CVF Winter Conference on Applications of Computer Vision (WACV)*, pages 692–701, 2023.
- [14] Yuk Heo, Yeong Jun Koh, and Chang-Su Kim. Interactive video object segmentation using global and local transfer modules. In *CVF Conference on European Conference on Computer Vision (ECCV)*, pages 297–313. Springer, 2020.
- [15] Alex Holub, Pietro Perona, and Michael C Burl. Entropy-based active learning for object recognition. In *IEEE/CVF Conference on Computer Society Conference on Computer Vision and Pattern Recognition Workshops*, pages 1–8. IEEE, 2008.

- [16] Chao Jia, Yinfei Yang, Ye Xia, Yi-Ting Chen, Zarana Parekh, Hieu Pham, Quoc V. Le, Yunhsuan Sung, Zhen Li, and Tom Duerig. Scaling up visual and vision-language representation learning with noisy text supervision. In *International Conference on Machine Learning (ICML)*, 2021.
- [17] Muhammad Uzair Khattak, Hanoona Rasheed, Muhammad Maaz, Salman Khan, and Fahad Shahbaz Khan. Maple: Multi-modal prompt learning. In *IEEE/CVF Conference on Computer Vision and Pattern Recognition (CVPR)*, 2023.
- [18] Mehar Khurana, Neehar Peri, James Hays, and Deva Ramanan. Shelf-supervised cross-modal pre-training for 3d object detection. *arXiv preprint arXiv:2406.10115*, 2024.
- [19] Alexander Kirillov, Eric Mintun, Nikhila Ravi, Hanzi Mao, Chloe Rolland, Laura Gustafson, Tete Xiao, Spencer Whitehead, Alexander C Berg, Wan-Yen Lo, et al. Segment anything. In *IEEE/CVF Conference on Computer Vision and Pattern Recognition (CVPR)*, pages 4015–4026, 2023.
- [20] Andreas Kirsch, Joost Van Amersfoort, and Yarin Gal. Batchbald: Efficient and diverse batch acquisition for deep bayesian active learning. *Advances in neural information processing systems*, 32, 2019.
- [21] Zhiqi Li, Wenhai Wang, Hongyang Li, Enze Xie, Chonghao Sima, Tong Lu, Qiao Yu, and Jifeng Dai. Bevformer: learning bird’s-eye-view representation from lidar-camera via spatiotemporal transformers. *IEEE Transactions on Pattern Analysis and Machine Intelligence*, 2024.
- [22] Tsung-Yi Lin, Michael Maire, Serge J. Belongie, James Hays, Pietro Perona, Deva Ramanan, Piotr Dollár, and C. Lawrence Zitnick. Microsoft COCO: common objects in context. In *CVF Conference on European Conference on Computer Vision (ECCV)*, 2014.
- [23] Zhiqiu Lin, Samuel Yu, Zhiyi Kuang, Deepak Pathak, and Deva Ramanan. Multimodality helps unimodality: Cross-modal few-shot learning with multimodal models. In *IEEE/CVF Conference on Computer Vision and Pattern Recognition (CVPR)*, 2023.
- [24] Haotian Liu, Chunyuan Li, Qingyang Wu, and Yong Jae Lee. Visual instruction tuning. In *Advances in Neural Information Processing Systems (NeurIPS)*, 2023.
- [25] Shilong Liu, Zhaoyang Zeng, Tianhe Ren, Feng Li, Hao Zhang, Jie Yang, Chunyuan Li, Jianwei Yang, Hang Su, Jun Zhu, et al. Grounding dino: Marrying dino with grounded pre-training for open-set object detection. *arXiv preprint arXiv:2303.05499*, 2023.
- [26] Tian Liu, Huixin Zhang, Shubham Parashar, and Shu Kong. Few-shot recognition via stage-wise retrieval-augmented finetuning. In *IEEE/CVF Conference on Computer Vision and Pattern Recognition (CVPR)*, 2025.
- [27] Pan Lu, Hritik Bansal, Tony Xia, Jiacheng Liu, Chunyuan Li, Hannaneh Hajishirzi, Hao Cheng, Kai-Wei Chang, Michel Galley, and Jianfeng Gao. Mathvista: Evaluating mathematical reasoning of foundation models in visual contexts. *arXiv preprint arXiv:2310.02255*, 2023.
- [28] Anish Madan, Neehar Peri, Shu Kong, and Deva Ramanan. Revisiting few-shot object detection with vision-language models. In *Advances in Neural Information Processing Systems (NeurIPS)*, 2024.
- [29] Maxime Oquab, Timothée Darcet, Théo Moutakanni, Huy Vo, Marc Szafraniec, Vasil Khalidov, Pierre Fernandez, Daniel Haziza, Francisco Massa, Alaaeldin El-Nouby, et al. Dinov2: Learning robust visual features without supervision. *arXiv:2304.07193*, 2023.
- [30] Aljovsa Ovsep, Tim Meinhardt, Francesco Ferroni, Neehar Peri, Deva Ramanan, and Laura Leal-Taixé. Better call sal: Towards learning to segment anything in lidar. In *CVF Conference on European Conference on Computer Vision (ECCV)*, pages 71–90. Springer, 2024.
- [31] Shubham Parashar, Zhiqiu Lin, Yanan Li, and Shu Kong. Prompting scientific names for zero-shot species recognition. In *Empirical Methods in Natural Language Processing (EMNLP)*, 2023.
- [32] Shubham Parashar, Zhiqiu Lin, Tian Liu, Xiangjue Dong, Yanan Li, Deva Ramanan, James Caverlee, and Shu Kong. The neglected tails in vision-language models. In *IEEE/CVF Conference on Computer Vision and Pattern Recognition (CVPR)*, pages 12988–12997, 2024.
- [33] Neehar Peri, Achal Dave, Deva Ramanan, and Shu Kong. Towards long-tailed 3d detection. In *Conference on Robot Learning (CoRL)*, pages 1904–1915. PMLR, 2023.
- [34] Nan Qiao, Yuyin Sun, Chong Liu, Lu Xia, Jiajia Luo, Ke Zhang, and Cheng-Hao Kuo. Human-in-the-loop video semantic segmentation auto-annotation. In *IEEE/CVF Winter Conference on Applications of Computer Vision (WACV)*, pages 5881–5891, 2023.

- [35] Alec Radford, Jong Wook Kim, Chris Hallacy, Aditya Ramesh, Gabriel Goh, Sandhini Agarwal, Girish Sastry, Amanda Askell, Pamela Mishkin, Jack Clark, et al. Learning transferable visual models from natural language supervision. In *International Conference on Machine Learning (ICML)*, pages 8748–8763. PMLR, 2021.
- [36] Deva Ramanan and David Forsyth. Automatic annotation of everyday movements. *Advances in neural information processing systems*, 16, 2003.
- [37] Pengzhen Ren, Yun Xiao, Xiaojun Chang, Po-Yao Huang, Zhihui Li, Brij B Gupta, Xiaojiang Chen, and Xin Wang. A survey of deep active learning. *ACM computing surveys (CSUR)*, 54(9):1–40, 2021.
- [38] Tianhe Ren, Shilong Liu, Ailing Zeng, Jing Lin, Kunchang Li, He Cao, Jiayu Chen, Xinyu Huang, Yukang Chen, Feng Yan, et al. Grounded sam: Assembling open-world models for diverse visual tasks. *arXiv:2401.14159*, 2024.
- [39] Md Alimoor Reza, Eric Manley, Sean Chen, Sameer Chaudhary, and Jacob Elafros. Segbuilder: A semi-automatic annotation tool for segmentation. In *IEEE/CVF Winter Conference on Applications of Computer Vision (WACV)*, pages 8494–8503. IEEE, 2025.
- [40] Victor Garcia Satorras and Joan Bruna Estrach. Few-shot learning with graph neural networks. In *International Conference on Learning Representations (ICLR)*, 2018.
- [41] Erich Schubert, Jörg Sander, Martin Ester, Hans Peter Kriegel, and Xiaowei Xu. Dbscan revisited, revisited: why and how you should (still) use dbscan. *ACM Transactions on Database Systems (TODS)*, 42(3):1–21, 2017.
- [42] Burr Settles. Active learning literature survey. *University of Wisconsin-Madison Department of Computer Sciences*, 2009.
- [43] Qianqian Shen, Yunhan Zhao, Nahyun Kwon, Jeeun Kim, Yanan Li, and Shu Kong. Solving instance detection from an open-world perspective. In *IEEE/CVF Conference on Computer Vision and Pattern Recognition (CVPR)*, 2025.
- [44] Julio Silva-Rodriguez, Sina Hajimiri, Ismail Ben Ayed, and Jose Dolz. A closer look at the few-shot adaptation of large vision-language models. In *IEEE/CVF Conference on Computer Vision and Pattern Recognition (CVPR)*, 2024.
- [45] Jake Snell, Kevin Swersky, and Richard Zemel. Prototypical networks for few-shot learning. *Advances in Neural Information Processing Systems*, 2017.
- [46] Pei Sun, Henrik Kretzschmar, Xerxes Dotiwalla, Aurelien Chouard, Vijaysai Patnaik, Paul Tsui, James Guo, Yin Zhou, Yuning Chai, Benjamin Caine, et al. Scalability in perception for autonomous driving: Waymo open dataset. In *IEEE/CVF Conference on Computer Vision and Pattern Recognition (CVPR)*, pages 2446–2454, 2020.
- [47] Yuwei Tang, Zhenyi Lin, Qilong Wang, Pengfei Zhu, and Qinghua Hu. Amu-tuning: Effective logit bias for clip-based few-shot learning. In *IEEE/CVF Conference on Computer Vision and Pattern Recognition (CVPR)*, 2024.
- [48] Gemini Team, Rohan Anil, Sebastian Borgeaud, Jean-Baptiste Alayrac, Jiahui Yu, Radu Soricut, Johan Schalkwyk, Andrew M Dai, Anja Hauth, Katie Millican, et al. Gemini: a family of highly capable multimodal models. *arXiv preprint arXiv:2312.11805*, 2023.
- [49] Hugo Touvron, Matthieu Cord, and Hervé Jégou. Deit iii: Revenge of the vit. In *CVF Conference on European Conference on Computer Vision (ECCV)*, 2022.
- [50] Xin-Jing Wang, Lei Zhang, Feng Jing, and Wei-Ying Ma. Annosearch: Image auto-annotation by search. In *IEEE/CVF Conference on Computer Vision and Pattern Recognition (CVPR)*, volume 2, pages 1483–1490. IEEE, 2006.
- [51] XuDong Wang, Jingfeng Yang, and Trevor Darrell. Segment anything without supervision. In *Advances in Neural Information Processing Systems (NeurIPS)*, 2024.
- [52] Benjamin Wilson, William Qi, Tanmay Agarwal, John Lambert, Jagjeet Singh, Siddhesh Khandelwal, Bowen Pan, Ratnesh Kumar, Andrew Hartnett, Jhony Kaesemodel Pontes, Deva Ramanan, Peter Carr, and James Hays. Argoverse 2: Next generation datasets for self-driving perception and forecasting. In *Proceedings of the Neural Information Processing Systems Track on Datasets and Benchmarks (NeurIPS Datasets and Benchmarks)*, 2021.

- [53] Benjamin Wilson, William Qi, Tanmay Agarwal, John Lambert, Jagjeet Singh, Siddhesh Khandelwal, Bowen Pan, Ratnesh Kumar, Andrew Hartnett, Jhony Kaesemodel Pontes, et al. Argoverse 2: Next generation datasets for self-driving perception and forecasting. *arXiv preprint arXiv:2301.00493*, 2023.
- [54] Aotian Wu, Pan He, Xiao Li, Ke Chen, Sanjay Ranka, and Anand Rangarajan. An efficient semi-automated scheme for infrastructure lidar annotation. *IEEE Transactions on Intelligent Transportation Systems*, 2024.
- [55] Hai Wu, Shijia Zhao, Xun Huang, Chenglu Wen, Xin Li, and Cheng Wang. Commonsense prototype for outdoor unsupervised 3d object detection. In *IEEE/CVF Conference on Computer Vision and Pattern Recognition (CVPR)*, pages 14968–14977, 2024.
- [56] Haoning Wu, Zicheng Zhang, Erli Zhang, Chaofeng Chen, Liang Liao, Annan Wang, Chunyi Li, Wenxiu Sun, Qiong Yan, Guangtao Zhai, et al. Q-bench: A benchmark for general-purpose foundation models on low-level vision. *arXiv preprint arXiv:2309.14181*, 2023.
- [57] Tianwei Yin, Xingyi Zhou, and Philipp Krahenbuhl. Center-based 3d object detection and tracking. In *IEEE/CVF Conference on Computer Vision and Pattern Recognition (CVPR)*, 2021.
- [58] Hao Zhang, Feng Li, Shilong Liu, Lei Zhang, Hang Su, Jun Zhu, Lionel Ni, and Harry Shum. Dino: Detr with improved denoising anchor boxes for end-to-end object detection. In *International Conference on Learning Representations (ICLR)*, 2022.
- [59] Lunjun Zhang, Anqi Joyce Yang, Yuwen Xiong, Sergio Casas, Bin Yang, Mengye Ren, and Raquel Urtasun. Towards unsupervised object detection from lidar point clouds. In *IEEE/CVF Conference on Computer Vision and Pattern Recognition (CVPR)*, pages 9317–9328, 2023.
- [60] Renrui Zhang, Rongyao Fang, Peng Gao, Wei Zhang, Kunchang Li, Jifeng Dai, Yu Qiao, and Hongsheng Li. Tip-adapter: Training-free adaption of clip for few-shot classification. In *CVF Conference on European Conference on Computer Vision (ECCV)*, 2022.
- [61] Renrui Zhang, Xiangfei Hu, Bohao Li, Siyuan Huang, Hanqiu Deng, Yu Qiao, Peng Gao, and Hongsheng Li. Prompt, generate, then cache: Cascade of foundation models makes strong few-shot learners. In *IEEE/CVF Conference on Computer Vision and Pattern Recognition (CVPR)*, 2023.
- [62] Wanjun Zhong, Ruixiang Cui, Yiduo Guo, Yaobo Liang, Shuai Lu, Yanlin Wang, Amin Saied, Weizhu Chen, and Nan Duan. Agieval: A human-centric benchmark for evaluating foundation models. *arXiv preprint arXiv:2304.06364*, 2023.
- [63] Jinghao Zhou, Chen Wei, Huiyu Wang, Wei Shen, Cihang Xie, Alan Yuille, and Tao Kong. Image bert pre-training with online tokenizer. In *International Conference on Learning Representations (ICLR)*, 2022.
- [64] Yijie Zhou, Likun Cai, Xianhui Cheng, Zhongxue Gan, Xiangyang Xue, and Wenchao Ding. Openannotate3d: Open-vocabulary auto-labeling system for multi-modal 3d data. In *IEEE Conference on Robotics and Automation (ICRA)*, pages 9086–9092. IEEE, 2024.

# Supplemental Document

This document supplements the main paper. Below is the outline of this document.

- **Section A** provides more discussions on broader impacts and limitations.
- **Section B** provides more details in refining 2D detectors.
- **Section C** provides details in heuristic LiDAR grouping.
- **Section D** provides LiDAR sensor matters in transfer learning.
- **Section E** provides details of training CenterPoint on AV2 dataset.
- **Section F** provides more details in 3D cuboid generation via MHT.
- **Section G** provides more details in different 3D generation methods.
- **Section H** studies how to refine dimension with guidelines.
- **Section I** displays more visual results.
- **Section J** provide image examples (training images for foundational 2D detector) in guidelines .
- **Section K** provides open-source code and more experimental details.

## A More Discussions

**Broader Impacts.** Although we commonly believe that pretraining on large-scale data will be the key enabler for generalization to open-world applications, understanding how to appropriately benchmark such methods and pretrained foundation models (FMs) remains challenging. FMs have been benchmarked in various ways through general tasks such as reasoning, math, open question answering, and physical rule understanding. Our AnnoGuide benchmark offers a new venue where various FMs can be accessed in multiple aspects with the final goal of 3D LiDAR detection, e.g., understanding textual descriptions in annotation guidelines, summarizing core information from texts and visual examples, generalizing to specific object classes for precise detection, etc. Our benchmark can facilitate the development of methods for automating data annotation by learning from expert-crafted guidelines. The developed methods can benefit real-world applications which adopt machine learning solutions, where data annotation is typically a prerequisite. Such applications span industry, health care, interdisciplinary research, etc. In the meanwhile, insights, philosophical thoughts and techniques delivered in this work may potentially inspire dataset curation and methods for malicious attacks for specific applications. These could be negative impacts.

**Limitations.** We note several limitations. First, while our pipeline demonstrates promising results, its real-world applicability for data annotation requires further comprehensive validation. Second, our methods do not leverage unlabeled data, which could be exploited through semi-supervised learning to enhance FM adaptation for AnnoGuide. Third, we rely on per-category size priors; adapting these priors to individual instances could further improve performance. Fourth, our tracking-based score refinement focuses on cuboid confidence but could also be used for optimizing cuboid orientation or velocity, which are key factors for autonomous driving and evaluation metrics like NDS. Fifth, our 3D cuboid generation operates on isolated object instances, but incorporating contextual and proxemic relationships between objects could yield additional gains. Finally, our work does not attempt to build a LiDAR-based foundation model, a critical yet underexplored direction for future research.

**Remarks on Expert-in-the-loop vs. human-in-the-loop.** AnnoGuide does not necessarily mean fully automated annotation without human intervention. Instead, it requires “expert-in-the-loop”, e.g., experts design not only the guidelines but also the pipeline for exploiting FMs towards automated data annotation. This is different from human-in-the-loop, which typically means that ordinary human annotators are involved in data annotation. Our work reveals that achieving AnnoGuide requires expert-in-the-loop, i.e., experts must design methods to adapt FMs to improve 2D detection and segmentation, and design geometric constraints. While it is reasonable to expect expert intervention in a highly specialized task, the lack of LiDAR-based FMs is another reason.

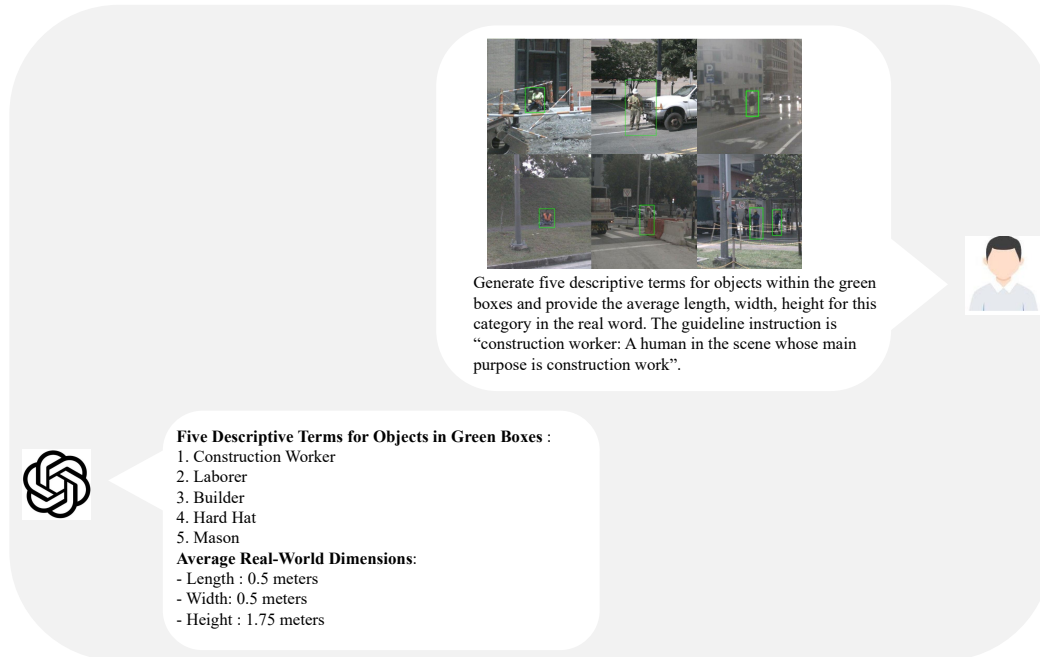


Figure 7: **Prompt generation workflow.** Visual examples from construction-worker annotation guidelines (green bounding boxes with local magnification and multi-view image mosaicing) are combined with textual instructions to derive enhanced prompts for GroundingDINO [25] via GPT-4o [2].

## B More Details in Refining 2D Detectors

**Prompt Refinement.** Our method enhances the generalization of a foundational 2D detector through three steps: (1) Visual enhancement: Localize targets with green bounding boxes and apply local magnification shown in Figure 2; (2) Structured Instruction: Generate prompts  $\{s_1, \dots, s_5\}$  and size prior  $(l_0, w_0, h_0)$  for each class via VLM with the template: “Generate five descriptive terms for objects within the green boxes and provide the average length, width, and height for this category in the real world. The guideline instruction is: [instruction].”, where [instruction] is replaced by actual guideline descriptions shown in Figure 7; (3) Efficient Validation: mirroring real-world annotation quality control practices (inspectors typically evaluate with minimal samples), we test randomly combined prompts on a minimal validation subset to identify the optimal multi-prompt composition. Based on the above stages, we get the best prompt for the foundational 2D detector shown in Table 6. It is important to note that while we employ GPT-4o [2] as the VLM for prompt refinement, alternative open-source VLMs such as QWen [3] can also be utilized for this purpose. We observe that QWen produces similar refined prompts, presumably that some terms are more frequent for a given class name that pretrained VLMs are more familiar with them so VLMs prefer to use these frequent terms [32].

**Few-Shot Finetuning the Foundation 2D detector.** Given the limited training data in annotation guidelines, we implement multiple augmentation strategies (e.g., random rotation and crop). Notably, the training images can be thought of as federated labeled data [28], i.e., an image is exclusively annotated with a specific class only. Therefore, we propose finetuning the 2D detector by focusing on the targeted class only for a training image and masking out other classes. We also use a small validation set for model selection and hyperparameter tuning. To construct a validation set, we randomly select 30 images per class from the nuScenes official validation set. The validation set can be thought of as a simulation of expert intervention in real-world annotation scenarios, where experts are overseeing annotation progress and quality, offering timely intervention when needed.

**Detailed Results.** Our main paper compares different foundational 2D detectors (finetuned vs. off-the-shelf), using different prompts (refined prompts vs. original class names). We now provide per-category results in Table 7: ft-GD using r-name gets the best results in 12/18 categories in 3D mAP metric, achieving significant improvements over the zero-shot baseline “GD (o-name)”, e.g., on

Table 6: **Mapping between the Original Class Names and the Best Prompts.** Notable combinatorial prompts occur in some categories (e.g., the best prompt of pushable-pullable is “pushable pullable garbage container” and “hand truck”).

The original class name	The refined class name
car	car
truck	truck
trailer	trailer, container
bus	bus
construction-vehicle	construction-vehicle
bicycle	bicycle bike
motorcycle	narrow motorcycle
emergency-vehicle	police vehicle, emergency vehicle
adult	adult
child	single little short youth children
police-officer	law enforcement officer
construction-worker	construction worker, laborer
stroller	stroller
personal-mobility	personal-mobility, small kick scooter
pushable-pullable	pushable pullable garbage container, hand truck
debris	debris, full trash bags
traffic-cone	traffic_cone
barrier	barrier

Table 7: More detailed (per-category) comparisons of results for different strategies of finetuning foundational 2D detectors yield different 3D detection performances. We report the results of zero-shot detector Detic as a reference, which is used in [18].

class	Detic (o-name)		GD (o-name)		ft-GD (o-name)		GD (r-name)		ft-GD (r-name)	
	mAP <sup>2D</sup>	mAP <sup>3D</sup>								
car	58.3	31.9	52.6	25.1	56.4	29.1	51.3	26.1	54.2	25.6
truck	37.2	17.6	34.3	14.2	34.4	15.0	36.3	14.1	37.5	12.6
trailer	4.2	0.8	8.5	2.0	7.0	1.3	8.1	1.8	8.5	1.7
bus	59.0	6.4	59.0	5.7	60.2	8.3	59.7	5.3	59.8	6.4
construction-vehicle	11.1	14.7	9.9	9.7	4.5	12.0	10.2	8.9	11.0	9.5
bicycle	28.8	28.6	22.4	22.7	28.5	27.5	22.5	19.6	24.2	29.5
motorcycle	38.1	50.9	21.7	42.0	36.4	48.1	20.8	33.5	31.5	50.0
emergency-vehicle	0.5	0.18	1.6	0.9	4.3	2.4	11.9	1.5	14.2	2.6
adult	10.2	5.6	23.5	54.4	36.9	53.8	23.9	53.8	31.8	58.8
child	0.0	0.00	0.9	0.8	1.1	0.7	6.6	3.2	5.2	3.5
police-officer	0.0	0.1	0.0	1.7	0.3	0.7	0.3	1.0	0.8	2.2
construction-worker	0.4	2.0	5.1	27.8	9.2	28.4	4.2	28.2	5.9	25.7
stroller	1.2	7.0	13.1	27.8	13.5	20.4	14.4	29.3	15.3	21.4
personal-mobility	0.0	0.0	0.0	0.0	0.0	0.0	0.9	0.7	10.6	9.4
pushable-pullable	0.0	0.0	2.6	1.2	2.9	1.1	6.1	2.8	5.8	4.8
debris	0.0	0.0	0.0	0.0	0.0	0.0	0.0	0.0	0.1	0.1
traffic-cone	51.8	50.5	46.2	44.2	52.7	40.1	46.9	43.4	52.5	52.0
barrier	0.8	0.6	3.6	9.7	2.8	8.5	2.8	8.5	5.9	11.4
avg.	16.5	12.1	16.9	16.1	20.0	16.6	18.2	15.7	<b>20.8</b>	<b>18.2</b>
NDS	16.6		21.3		21.2		22.1		<b>23.1</b>	

adult (54.4 to 58.8), personal-Mobility (0.0 to 9.4), motorcycle (42.0 to 50.0), traffic-cone (44.2 to 52.0).

## C Details in Heuristic LiDAR Grouping

In this project, for 3D cuboid generation, we designed a heuristic method which clusters LiDAR points (in a specific frustum) towards an object instance based on point density. Given a frustum of point cloud corresponding to a 2D detection, we find the largest cluster  $\mathcal{C} = \{\mathbf{p}_i\}_{i=1}^N$  via density-based clustering. The 3D center  $\mathbf{c} = (x, y, z)$  is computed as:

$$\mathbf{c} = \frac{1}{N} \sum_{i=1}^N \mathbf{p}_i \quad (1)$$

Box dimensions  $(l, w, h)$  are derived from cluster boundaries:

$$l = \max(\mathcal{C}_x) - \min(\mathcal{C}_x), \quad w = \max(\mathcal{C}_y) - \min(\mathcal{C}_y), \quad h = \max(\mathcal{C}_z) - \min(\mathcal{C}_z) \quad (2)$$

The yaw angle  $\theta$  is estimated via multi-frame trajectory. For consecutive centers  $\mathbf{c}_t, \mathbf{c}_{t+\Delta t}$ :

$$\theta = \arctan\left(\frac{y_{t+\Delta t} - y_t}{x_{t+\Delta t} - x_t}\right) \quad (3)$$

We compare this heuristic clustering method in Table 9.

## D LiDAR Sensor Matters in Transfer Learning

We tested a model purposefully trained on another dataset, Argoverse2 (AV2) to investigate whether LiDAR-based pretrained models can generalize to specific domains of interest. We train a 3D detector CenterPoint (CP) on the AV2 dataset (detailed in the next section), but this model exhibits severe performance degradation on the nuScenes benchmark (see CP results in Table 2 and Table 9). Our analysis of LiDAR sensor parameters (Table 8) reveals significant discrepancies between LiDAR sensors of the two datasets: (1) measurement range, (2) horizontal/vertical FOV, (3) point cloud density, and (4) intensity sensitivity. We conjecture the discrepancies explain the difficulty of transferring 3D detectors pretrained on different LiDAR sensors.

Table 8: **Specifics of different LiDAR sensors in nuScenes and Argoverse2 (AV2) for data collection.** Clearly, the LiDAR sensors notably differ in measurement range, horizontal/vertical FOV, point cloud density, and vertical distribution patterns.

parameter/feature	LiDAR Configuration	
	nuScenes [8]	AV2 [52]
LiDAR Model	Single HDL-32E	Dual VLP-32C
Number of channels	32	$32 \times 2$
Measurement Range	Max 100m, Effective 70m	Max 200m, Effective 100m
Vertical FOV	-30.67° to + 10.67°	-25° to + 15°
Horizontal FOV	360°	360°
Scan Frequency	20Hz	10Hz
Points per Second	~600k pts/s (20Hz $\times$ 30k/frame)	~1.2M pts/s (10Hz $\times$ 120k/frame $\times$ 2)
Vertical Resolution	0.4° (center), 0.4° to 2.08° (edge)	0.33° (center), 1.0° (edge)
Horizontal Resolution	0.32° (20Hz)	0.096° (10Hz)
Intensity Range	0-255	0-255

## E Details of Training CenterPoint on AV2 Dataset

Since the AV2 dataset provides fine-grained category annotations, we train a 3D detector (CenterPoint in this paper) on AV2, where the point cloud data includes multi-dimensional features including  $x$ ,  $y$ ,  $z$  coordinates, intensity, timestamp, and laser number, forming  $N \times 5$  input features ( $N$  denotes the number of points). After training on AV2, we adapt the nuScenes dataset to the same format. However, as discussed in Section D, the differences exist between the two datasets about intensity sensitivity, acquisition frequency, and LiDAR channel distribution in the input features. For category name alignment, we project 3D detections to image plane as 2D boxes  $\mathcal{B}_{3D}$ , compute IoU with 2D detections  $\mathcal{B}_{2D}$  via:

$$\text{IoU} = \frac{|\mathcal{B}_{3D} \cap \mathcal{B}_{2D}|}{|\mathcal{B}_{3D} \cup \mathcal{B}_{2D}|} \quad (4)$$

and assign semantic labels through maximum IoU matching strategy.

## F More Details in 3D Cuboid Generation via MHT

We first cluster object points using DBSCAN [41] and retain the largest cluster, eliminating noisy projections (e.g., walls behind the object). We fix the 3D dimensions  $(l_0, w_0, h_0)$  obtained from VLM (GPT-4o [2] in our experiment) and initialize the 3D cuboid center at the cluster centroid. During sliding optimization, we adjust parameters  $\theta = [x, y, z, \psi]$  (3D center + orientation) and compute the in-cuboid point ratio:

$$R(\theta) = \frac{1}{|P|} \sum_{p_i \in P} \mathbb{I}(p_i \in B_{3D}), \quad (5)$$

where  $P$  is the denoised point cluster,  $\mathbb{I}(\cdot)$  is the indicator function, and  $B_{3D}$ ,  $B_{2D}$  represent the 3D cuboid and 2D detection bounding boxes, respectively. When multiple candidates share equal  $R(\theta)$ , we select:

$$\theta^* = \arg \max_{\theta} \text{IoU}(\pi(B_{3D}(\theta)), B_{2D}), \quad (6)$$

where  $\pi(\cdot)$  implements perspective projection using camera parameters.

## G More Details in Different 3D Generation Methods

Table 9 extends the 3D cuboid generation analysis in our main paper with per-category results. Our MHT-based approach (Fig. 5) demonstrates particular advantages in vehicle categories, improving AP by 4.4% (car), 2.8% (truck), and 7.6% (bus) over CM3D [18].

## H 3D Few-Shot Dimension Refinement with Guidelines

We design a PointNet-based lightweight network  $P_{\phi}$  in Fig. 8 to refine the dimensions of the objects  $(l_0, w_0, h_0)$  using limited 3D annotation for each category, where the input features are constructed by 3D rigid transformation. The raw points  $\mathbf{p}_{\text{raw}} = (x, y, z)$  are transformed into a local coordinate system centered on the centroid of the 3D proposal  $(x_0, y_0, z_0)$  with the x-axis aligned to yaw  $\theta_0$ , producing  $\mathbf{p}_{\text{trans}} = (x_{\text{trans}}, y_{\text{trans}}, z_{\text{trans}})$ . The input feature  $\mathcal{F} \in \mathbb{R}^{N \times 9}$  concatenates three components: transformed coordinates  $\mathbf{p}_{\text{trans}}$ , differences  $\mathbf{d}_0 - \mathbf{p}_{\text{trans}}$ , and sums  $\mathbf{d}_0 + \mathbf{p}_{\text{trans}}$ :

$$\mathcal{F} = [\mathbf{p}_{\text{trans}}, (\mathbf{d}_0 - \mathbf{p}_{\text{trans}}), (\mathbf{d}_0 + \mathbf{p}_{\text{trans}})] \quad (\mathbf{d}_0 = (l_0, w_0, h_0)) \quad (7)$$

where the coordinate transformation is defined as:

$$\mathbf{p}_{\text{trans}} = \begin{bmatrix} \cos \theta_0 & \sin \theta_0 & 0 \\ -\sin \theta_0 & \cos \theta_0 & 0 \\ 0 & 0 & 1 \end{bmatrix} \left( \mathbf{p}_{\text{raw}} - \begin{bmatrix} x_0 \\ y_0 \\ z_0 \end{bmatrix} \right). \quad (8)$$

The network  $P_{\phi}$  predict log-scale offsets between ground-truth dimensions  $l_{\text{gt}}, w_{\text{gt}}, h_{\text{gt}}$  and initial values  $l_0, w_0, h_0$  by VLM:

$$\Delta l = \log \left( \frac{l_{\text{gt}}}{l_0} \right), \quad \Delta w = \log \left( \frac{w_{\text{gt}}}{w_0} \right), \quad \Delta h = \log \left( \frac{h_{\text{gt}}}{h_0} \right), \quad (9)$$

and using Smooth L1 loss jointly optimizes all three axes:

$$\mathcal{L} = \sum_{\Delta d \in \{\Delta l, \Delta w, \Delta h\}} \text{SmoothL1}(\Delta d). \quad (10)$$

This architecture corrects fixed dimensions, improving detection metrics even with scarce 3D annotation.

## I More Visualizations

Fig. 9 visualizes more visual results on the nuScenes dataset [8].

## J Image Examples in Guidelines

Fig. 10 illustrates example images of 5 categories from the guidelines (3 examples visualized per category), where the green bounding boxes represent the 2D projections of the 3D annotations. The complete set of image examples can be found in the supplementary material. These image examples serve as training data for finetuning the foundational 2D detector.

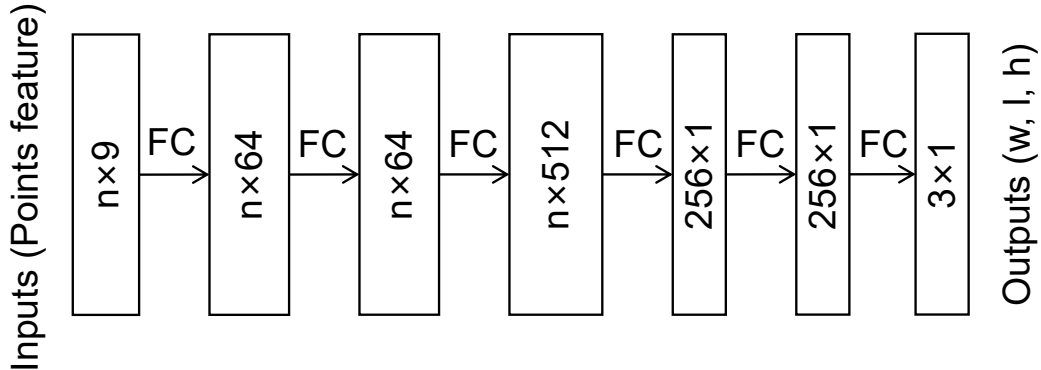


Figure 8: **Architecture of lightweight regression network.** The input features with dimension  $n \times 9$  ( $n$ : number of LiDAR points in 3D proposal, 9-channel features include shown in Eq. (7)) are processed to output  $n \times 3$  logarithmic offsets  $(\Delta l, \Delta w, \Delta h)$  for dimension refinement. It should be noted that each category uses an independently trained model due to limited data availability.

Table 9: Per-category results of different 3D cuboid generation methods.

Class	Heuristic Clustering	CM3D [18]	AV2-Pretrained CenterPoint	MHT
car	18.7	25.6	15.6	30.0
truck	10.2	12.6	4.1	15.4
trailer	0.8	1.7	0.2	1.7
bus	3.7	6.4	2.2	14.0
construction-vehicle	9.0	9.5	1.0	9.5
motorcycle	49.2	50.0	8.4	50.7
emergency-vehicle	2.6	2.6	0.2	5.4
adult	57.3	58.8	15.8	58.8
child	3.4	3.5	0.0	3.5
police-officer	2.0	2.2	2.0	2.2
construction-worker	25.8	25.7	3.6	25.7
stroller	20.8	21.4	0.4	21.5
personal-mobility	9.4	9.4	0.0	8.7
pushable-pullable	0.1	0.1	0.0	0.1
debris	0.1	0.1	0.0	0.1
traffic-cone	52.0	52.0	8.7	52.0
barrier	11.7	11.4	0.0	11.5
<b>mAP</b>	17.3	18.2	3.6	<b>19.2</b>
<b>NDS</b>	21.6	23.1	19.0	<b>23.8</b>

## K Open-Source Code and More Experimental Details

**Open-Source Code.** We include our codebase as a part of the supplementary material, refer to the zip README.md for instructions about how to run the code. We do not include model weights in the supplementary material as they exceed the space limit (100MB). We have polished a webpage (<https://annoguide.github.io/annoguide3Dbenchmark> and used GitHub to host our open-source code, models and results under the MIT License at: <https://github.com/annoguide/annoguide3Dbenchmark>

**More Experimental Details.** The training environment uses Python 3.8.20 with PyTorch 2.4.1+cu121 and 4 compute workers. We employ an AdamW optimizer (lr=0.0001, weight\_decay=0.0001) on a single NVIDIA A6000 GPU with 40GB memory, reaching peak GPU memory usage of 26GB when training GroundingDINO. The dataset of training GroundingDINO comprises 112 training images ( $\sim 6$  per class), 570 validation images ( $\sim 32$  per class), and 36114 test images (6,019 LiDAR frames  $\times 6$  images). End-to-end training GroundingDINO with online validation takes approximately 2 hours. For 3D bounding box generation, processing per LiDAR frame (6 images) requires 11 seconds on average: 9 seconds for GroundingDINO and SAM (1.5s per) and 2 seconds for 3D generator.

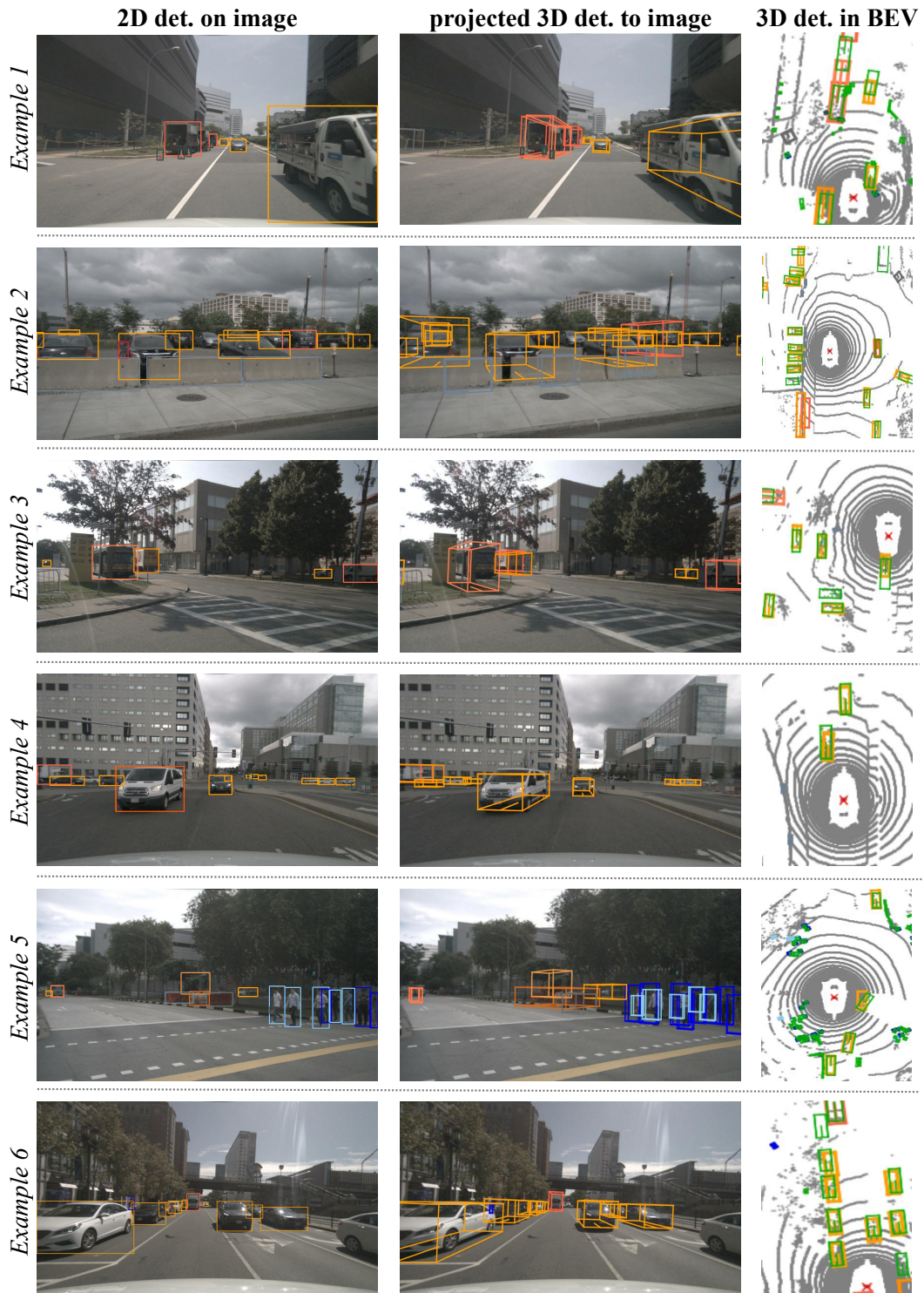


Figure 9: More visual results of automated 3D annotation.

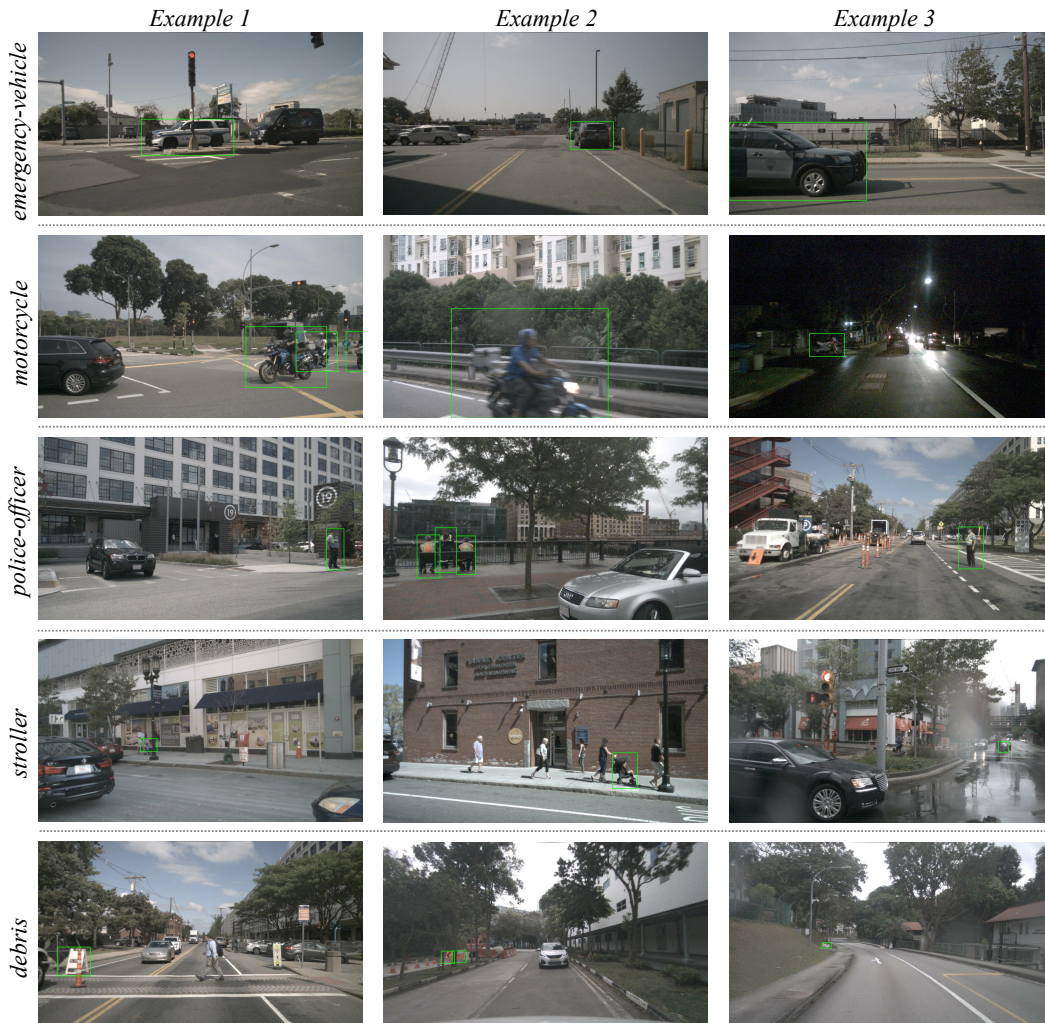


Figure 10: **Images examples in annotation guidelines.** We present 5 out of the 18 categories, with 3 example images shown for each category, where the green bounding boxes is projected from the 3D annotation cuboids into the image. It should be noted that, taking the `emergency-vehicle` category as an example, even if objects of the `car` category appear in the images, no corresponding annotations are provided.